

A Sub-kpc Disk in MRK 231

C.L. Carilli, J.M. Wrobel, J.S. Ulvestad

NRAO, P.O. Box O, Socorro, NM, 87801, USA

Received _____; accepted _____

To appear in the Astronomical Journal (accepted Nov. 26, 1997)

ABSTRACT

We present imaging with the Very Long Baseline Array of the neutral hydrogen 21cm absorption line system seen toward the nuclear regions of Mrk 231 at $z_{\odot} = 0.04217$, and imaging of the radio continuum emission at 1.4 GHz on scales ranging from a few parsecs to a few hundred parsecs. These data indicate the existence of a sub-kpc gas disk in Mrk 231, as seen in HI 21cm absorption and in radio continuum emission. The radio continuum morphology is consistent with a disk of maximum radius of 440 mas ($260 \text{ h}^{-1} \text{ pc}$), at an inclination angle of 45° , with a major axis oriented east-west. The HI 21cm absorption shows an east-west gradient in position and velocity of about $\pm 110 \text{ km s}^{-1}$ out to radii of 100 mas ($60 \text{ h}^{-1} \text{ pc}$). We identify this HI and radio continuum disk as the inner part of the molecular disk seen on a factor three larger scale. The physical conditions for the thermal and non-thermal gas in the sub-kpc disk of Mrk 231 are similar to those proposed for compact nuclear starburst galaxies, and in particular to the conditions proposed for the sub-kpc gas disk in Arp 220. From the neutral hydrogen velocity field we derive a gravitational mass enclosed within a $50 \text{ h}^{-1} \text{ pc}$ radius of $3 \times 10^8 \text{ h}^{-1} M_{\odot}$, and from the radio continuum emission we derive a massive star formation rate in the disk of $60 M_{\odot} \text{ year}^{-1}$.

We also present a search for HI 21cm absorption associated with the optical broad absorption line (BAL) systems toward Mrk 231. We do not detect HI 21cm absorption associated with any of the optical BAL systems. These negative results require that the neutral atomic gas in the BAL clouds be fairly warm ($T_s > 50 \text{ K}$), unless the NaI abundance is higher than solar, or the dust-to-gas ratio is higher than Galactic, or the observed extinction toward the nucleus of Mrk 231 is not due to the BAL gas.

Subject headings: galaxies:seyferts, active, ISM - quasars:absorption lines -
radio lines: galaxies

1. Introduction

The Seyfert 1 galaxy Mrk 231 has an infrared (IR) luminosity of $3 \times 10^{12} h^{-2} L_{\odot}$, making it the most luminous infrared galaxy in the sample of ultra-luminous infrared galaxies (ULIRGs) of Sanders et al. (1988).¹ Most of the infrared emission from Mrk 231 comes from a region less than $0.5''$ ($300 h^{-1} \text{ pc}$) in size (Matthews et al. 1987). Imaging of the CO emission from Mrk 231 by Bryant and Scoville (1996) shows a molecular disk on a scale of about $1''$. Deep optical imaging of Mrk 231 reveals a disturbed parent galaxy, perhaps with a weak secondary nucleus, and with clear tidal features indicating a merger within the last 10^9 years (Hamilton and Keel 1987, Hutchings and Neff 1987, Armus et al. 1994, Surace et al. 1997). Radio continuum imaging shows an active radio nucleus with a high surface brightness core plus radio lobes extending both north and south to about 30 mas (Ulvestad, Wrobel, and Carilli 1997a).

Sanders et al. (1988) have proposed that ultraluminous infrared galaxies are part of a sequence in which merging spiral galaxies evolve through a starburst phase, eventually becoming optical QSOs (see also Sanders and Mirabel 1996). The early stage of the merger (10^7 years) involves molecular cloud collisions, leading to a ‘funneling of the gas into the merger nucleus’. This gas then fuels a nuclear starburst on a timescale of about 10^8 years. An important mechanism in this sequence entails the ‘formation of a self-gravitating gas disk’ in the galaxy center on a scale $\leq 1 \text{ kpc}$. This disk would be dissipative, driving gas condensation further into the nucleus, and fueling the active nucleus. Radiation and/or winds from the active nucleus would eventually clear-out the obscuring material, revealing an optical QSO. Scoville, Yun, and Bryant (1997) show that the physical conditions in the disk may be conducive to star formation. Sanders et al. propose that Mrk 231 represents

¹We use $h \equiv \frac{H_0}{100} \text{ km s}^{-1} \text{ Mpc}^{-1}$, giving a scale of: $1 \text{ mas} = 0.6 h^{-1} \text{ pc}$ at the redshift of Mrk 231, $z = 0.042$.

a late stage in this process, namely the ‘dust enshrouded QSO’ stage. The origin of the massive black hole remains uncertain (Weedman 1983).

An important question concerning the Sanders et al. (1988) model is: do sub-kpc gas disks exist in ULIRGs? Such gas disks have been proposed in Mrk 231 and Arp 220, based on molecular imaging observations (Bryant and Scoville 1996, Scoville, Yun, and Bryant 1997). In this paper we present high resolution imaging of the neutral hydrogen 21cm absorption line system seen toward the nuclear regions of Mrk 231 (Heckman, Balick and Sullivan 1978, Dickey 1982), and of the radio continuum emission at 1.4 GHz on scales ranging from a few parsecs to a few hundred parsecs. These data support the existence of a sub-kpc gas disk in Mrk 231, as seen both in HI 21cm absorption and in radio continuum emission. These data also suggest that star formation activity may be significant in the disk.

We also present a search for HI 21cm absorption associated with the optical broad absorption line systems toward Mrk 231. One of the more interesting observations of Mrk 231 has been the detection of low ionization, time variable, broad absorption lines systems (BAL) toward the optical nucleus, with out-flow velocities of a few thousand km s^{-1} (Boksenberg et al. 1978, Boroson et al. 1991, Kollatschny, Deitric, and Hagen 1992, Forster et al. 1995). Boksenberg et al. (1978) suggest that much of the dust giving rise to the $A_V = 2$ toward the nucleus of Mrk 231 could be associated with these low ionization BAL clouds. We do not detect HI 21cm absorption associated with any of the BAL systems. These data provide interesting constraints on the physical conditions in the BAL gas seen toward Mrk 231.

2. Observations, Calibration, and Imaging

2.1. VLBA

Observations of Mrk 231 were made on December 27, 1996 with the Very Long Baseline Array (VLBA) operated by the National Radio Astronomy Observatory (NRAO; Napier et al. 1994). These observations included the phased Very Large Array (VLA) as an element in the very long baseline array. The VLA was in its largest (33 km) configuration. The pass band was centered at the frequency of the neutral hydrogen 21cm line at a heliocentric redshift of: $z = 0.04216$, or $cz = 12640 \text{ km s}^{-1}$. The total bandwidth was 8 MHz, using two orthogonal polarizations, 256 spectral channels, and 2 bit correlation.

All data reduction was performed using the Astronomical Image Processing System (AIPS) of the NRAO. Standard *a priori* gain calibration was performed using the measured gains and system temperatures of each antenna. The compact radio source J1219+48 was observed every 20 minutes, and this source was used to determine the fringe rates and delays during the observations. These solutions were then applied to the Mrk 231 data. The source 3C 345 (J1642+39) was used to calibrate the frequency dependent gains (band pass calibration). The source J1310+32 was used to check the absolute gain calibration, and to check the band pass calibration. The results showed agreement of observed and expected flux densities to within 10%, and bandpass calibration accuracy to better than 2% (peak-to-peak residual variations).

After application of the delay and rate solutions, and band pass calibration, a continuum data set for Mrk 231 was generated by averaging off-line channels. This continuum data set was then used for the hybrid imaging process, which involves iterative imaging and self-calibration of the antenna-based complex gains (Walker 1985). The final iteration involved both phase and amplitude calibration with a 1 minute averaging time. The self-calibration solutions were applied to the spectral line data set. The spectral line data were then analyzed at various spatial and spectral resolutions by tapering the visibility

data, and by smoothing in frequency. Standard analysis of the spectral line image cubes involved subtracting the continuum emission by fitting linear spectral baselines at each position to the off-line channels using the AIPS routine IMLIN, and then deconvolving the synthesized beam using the Clark ‘CLEAN’ algorithm as implemented in the AIPS routine APCLN (Clark 1980). The channel images were CLEANed to a residual level equal to twice the root mean square (rms) noise level.

2.2. VLA

Observations of Mrk 231 were made on January 27, 1993 with the VLA in the 10 km configuration (Napier, Thompson, and Ekers 1983), centered on the frequency of the neutral hydrogen 21cm line at the heliocentric redshifts of the three broad absorption line systems seen toward Mrk 231: $z = 0.01554$ ($cz = 4660 \text{ km s}^{-1}$), $z = 0.02085$ ($cz = 6250 \text{ km s}^{-1}$), and $z = 0.02668$ ($cz = 8000 \text{ km s}^{-1}$). One polarization was received, and on-line Hanning smoothing was applied. Observations at 4660 km s^{-1} and 6250 km s^{-1} used 63 spectral channels with a channel width of 97.6 kHz, while those at 8000 km s^{-1} used 31 spectral channels with a channel width of 390.6 kHz. Absolute gain, complex gain, and band pass calibration were performed on 3C 286. After application of the standard calibration solutions, a continuum data set was generated by averaging all channels, and this data set was used for iterative self-calibration of the antenna based complex gains (all the channels were used since no line signal was detected). The self-calibration solutions were then applied to the spectral line data. The continuum emission was then subtracted from the spectral line image cubes by fitting linear spectral baselines at each position to all the channels.

Observations of Mrk 231 were also made on August 31, 1997 with the VLA in the 3 km configuration, centered on the frequency of the neutral hydrogen 21cm line at the

heliocentric redshift of 0.04212 ($cz = 12640 \text{ km s}^{-1}$). Two orthogonal polarizations were received, with 63 spectral channels, with a channel width of 48.8 kHz, and on-line Hanning smoothing was applied. The data were calibrated, self-calibrated, and imaged as described above. We assume the errors in absolute gain calibration are 3% for the VLA observations (Carilli et al. 1991).

3. Results

3.1. Radio Continuum

The VLA image of Mrk 231 at 1.4 GHz at $5''$ resolution made from data taken in January 1993 is shown in Figure 1. The image shows a compact source with a peak surface brightness of $240 \pm 7 \text{ mJy beam}^{-1}$. There is also low surface brightness emission extending at least $30''$ to the south, and the total source flux density is $320 \pm 9 \text{ mJy}$. A detailed discussion of the very extended radio continuum emission from Mrk 231 is given in Ulvestad et al. (1997b). The VLA image from data taken in December 1996 shows a peak surface brightness of $230 \pm 8 \text{ mJy beam}^{-1}$ at $1.3''$ resolution, while the data taken on August 31, 1997 show a peak surface brightness of $242 \pm 8 \text{ mJy beam}^{-1}$. Hence, the variation of the central continuum source over this time period is less than 5% at 1.4 GHz.

The VLBA image of Mrk 231 at 1.4 GHz at 6 mas resolution is shown in Figure 2. The image shows a double source, with a compact central peak of $40 \pm 4 \text{ mJy beam}^{-1}$, and a ‘lobe’ extending 30 mas to the south with a total flux density of $44 \pm 5 \text{ mJy}$. There is also evidence for a fainter lobe extending about 20 mas to the north with a total flux density of about $4 \pm 1 \text{ mJy}$. This northern lobe has been detected at a number of frequencies in the sensitive VLBI continuum observations of Ulvestad et al. (1997a). The southern radio lobe is thought to be the approaching lobe, based on the observation of excess free-free

absorption toward the northern lobe (Ulvestad et al. 1997a). The total flux density of the source in this image is 100 ± 10 mJy. There is a low surface brightness ‘bridge’ connecting the central peak with the southern lobe, perhaps indicating a jet. A detailed discussion of the continuum emission on 10 mas scales from Mrk 231 is given in Ulvestad et al. (1997a).

The VLBA data also reveal the existence of diffuse emission on a scale considerably larger than the compact core and lobes seen in Figure 2. The shortest projected interferometer spacings of our VLBI experiment are about $180 \text{ k}\lambda$, where λ is the observing wavelength, corresponding to a resolution of about $1''$, and the source flux density increases to about 230 mJy on these spacings, comparable to the observed flux density on the longest VLA spacings. In order to determine the distribution of this diffuse emission, we subtracted the CLEAN component model of the source seen at high resolution in Figure 2 from the visibility data set, and we imaged the residual visibilities using a Gaussian taper with $\text{FWHM} = 3 \text{ M}\lambda$, corresponding to data primarily from the inner-most antennas of the array (the VLA, Pie Town, Los Alamos, and Fort Davis). The resulting image is shown in Figure 3 at a resolution of 60 mas. The image shows an elliptical source roughly centered on the core-lobe source, with a major axis of 440 mas oriented east-west, and a minor axis of 310 mas. The total flux density in this diffuse component is 130 ± 13 mJy. The average surface brightness in the inner 200 mas is $6 \pm 2 \text{ mJy beam}^{-1}$, corresponding to a brightness temperature of 10^6 K . The surface brightness then drops to about 3 mJy beam^{-1} at radii larger than 100 mas. From the longest spacings of the VLA we derive an upper limit of $0.5''$ to the size of this diffuse emission.

3.2. HI 21cm Absorption: Systemic Velocity

Figure 4 shows the HI 21cm absorption spectrum of Mrk 231 made with the VLA in August 1997 at a spectral resolution of 21 km s^{-1} and a spatial resolution of $18''$. The

continuum flux density of 242 ± 8 mJy has been subtracted, and the spectrum has been converted to optical depth using this continuum level. The rms noise (σ) in this spectrum is 0.8 mJy beam $^{-1}$ channel $^{-1}$. The peak absorbed flux density is -19 ± 1 mJy. A single Gaussian component fit to the absorption line results in a peak opacity of 0.083 ± 0.002 , and a velocity FWHM = 179 ± 5 km s $^{-1}$. The peak of the Gaussian fit is at a heliocentric redshift of 0.04217 ± 0.000015 , or $cz = 12642 \pm 4$ km s $^{-1}$. We adopt this redshift as the zero point in the velocity scale in this, and subsequent, spectra.

The most surprising results from this study are the HI 21cm absorption spectra toward the VLBI core and lobe components seen on 10 mas scales in Figure 2. These spectra are shown in Figure 5 at 56 km s $^{-1}$ resolution. The spectra were extracted at the position of the peak surface brightnesses of the two continuum components on images convolved to 13 mas resolution. The spectra have been converted to optical depth using the continuum surface brightnesses of 43 mJy beam $^{-1}$ for the peak, and 20 mJy beam $^{-1}$ for the southern lobe. The rms noise in these spectra is 0.3 mJy beam $^{-1}$ channel $^{-1}$. We expected to see strong absorption (as much as 19 mJy), either toward the nucleus or toward the southern lobe. However, no absorption is seen toward either of these components to a 3σ level of 1 mJy, or optical depth limits of 0.02 for the peak and 0.04 for the southern lobe. The faintness of the northern lobe only allows us to set a 3σ optical depth limit of 0.5 .

Spectral images were then synthesized by tapering the VLBI visibilities to look for absorption against the diffuse continuum emission seen on scales of a few hundred mas as shown in Figure 3. A spectrum made with a spatial resolution of 400 mas (comparable to the size of the diffuse radio continuum emission shown in Figure 3), and a spectral resolution of 28 km s $^{-1}$, is shown in Figure 6. The peak surface brightness is 91 mJy beam $^{-1}$ (after subtracting the contribution from the VLBI core and lobes). A strong HI 21cm absorption line is observed, with a peak flux density of -14 ± 2 mJy. A single Gaussian component fit

to the absorption line results in a peak opacity of 0.17 ± 0.02 , a velocity FWHM = 193 ± 25 km s⁻¹, and a velocity centroid of -21 ± 12 km s⁻¹.

Spectral channel images of the HI 21cm absorption toward the diffuse continuum emission from the central regions of Mrk 231 are shown in Figure 7 for images tapered to a spatial resolution of 150 mas, and smoothed to a spectral resolution of 58 km s⁻¹. The absorption shows a clear velocity gradient from west to east, starting at -130 km sec⁻¹ at 100 mas west of the continuum peak, and moving to $+100$ km sec⁻¹ at a comparable distance to the east of the continuum peak.

It is important to keep in mind that, unlike HI emission studies, HI absorption measurements depend both on the neutral gas distribution and the background continuum distribution. Hence it is difficult to determine whether the fading of the HI absorption signal to the east and west is due to the lack of HI or the lack of continuum. We find that the peak opacity is roughly constant across the brighter regions of the source, with a value of about 0.18 ± 0.04 to a distance of at least 100 mas both east and west of the nucleus. The continuum surface brightness beyond a radius of 100 mas is too low to detect absorption in the current data.

3.3. HI 21cm Absorption: The Broad Absorption Line Systems

Optical spectra of Mrk 231 have revealed broad absorption line systems at heliocentric velocities of: $cz = 4660$ km s⁻¹, 6250 km s⁻¹, and 8000 km s⁻¹ (Boroson et al. 1991, Forster et al. 1995, Rudy et al. 1985). The 4660 km s⁻¹ and 6250 km s⁻¹ systems have velocity widths of about 200 km s⁻¹, while the system at 8000 km s⁻¹ has a velocity width of about 1000 km s⁻¹. These systems show absorption by low ionization state species, such as NaI. Given that NaI atoms have a lower ionization potential than HI, one might hope to see

associated absorption in the 21cm line of neutral hydrogen.

Given the different velocity widths of the optical BAL systems, we observed the two lower redshift systems with a velocity resolution of 21 km s^{-1} , while the higher redshift system was observed with a velocity resolution of 87 km s^{-1} . The absorption spectra are shown in Figure 8. No absorption was detected in any of the systems. The spectral rms for the two lower redshift systems is $0.7 \text{ mJy channel}^{-1}$, while that in the spectrum of the higher redshift system is $0.6 \text{ mJy channel}^{-1}$. The continuum flux density is $240 \pm 7 \text{ mJy}$, hence the 3σ optical depth limits per spectral channel are 0.009 for the two lower redshift systems, and 0.008 for the higher redshift system.

4. Discussion

4.1. The Neutral Atomic Disk

The three important results from our high resolution imaging observations of the HI 21cm absorption at 12642 km s^{-1} toward Mrk 231 are that: (i) absorption is *not* seen toward the VLBI core and lobes, (ii) absorption is detected toward a diffuse, elliptical radio continuum component which is centered on the nucleus and has a maximum size of 440 mas ($= 260 \text{ h}^{-1} \text{ pc}$), and (iii) the absorption shows an east-west gradient in position and velocity of about $\pm 110 \text{ km s}^{-1}$ out to radii $\approx 100 \text{ mas}$ ($60 \text{ h}^{-1} \text{ pc}$). One plausible explanation of these three observed characteristics is that the neutral atomic gas, and the radio continuum emitting gas, are in a disk centered on the active galactic nucleus (AGN), and that the disk is oriented not too far from the sky plane, and that the radio lobe axis is oriented perpendicular to the disk. We discuss this model in the following section (see also Figure 9 and the discussion at the end of section 4.2).

Perhaps the strongest argument that the absorbing neutral hydrogen in Mrk 231 is in

a disk is the simple fact that such a gas disk has already been seen in the CO molecular line images of Bryant and Scoville (1996), and that the parameters for HI absorption are consistent with those of the molecular disk (see below). The molecular observations show an elliptical distribution for the CO, with a major axis of $1.2''$ oriented east-west and a minor axis of $0.8''$. The molecular gas shows an east-west velocity gradient, ie. along the disk major axis. The molecular disk model of Bryant and Scoville is based primarily on the fact that, if the molecular gas was spherically distributed about the nucleus, the gas mass would greatly exceed the dynamical mass. They set a conservative upper limit to the disk inclination angle relative to the sky plane of: $i < 59^\circ$. They also show that a spherical distribution would lead to an $A_V \approx 100$ toward the nucleus, in conflict with the observed value of $A_V \approx 2$ (Boksenberg et al. 1978).

The HI observations presented herein show an east-west velocity gradient for the atomic gas that is similar in both magnitude and position angle to that seen for the molecular disk, although on a factor three smaller scale. We would then identify the observed HI gas with the inner regions of the molecular disk seen in CO emission. We should emphasize that we cannot rule out an outflow model to explain the HI velocity gradient, as opposed to rotation. One argument against outflow is that the atomic and molecular gas outflow axis would then be perpendicular (at least in projection) to the radio jet outflow axis.

An HI disk not too far from the sky plane would provide a natural explanation for the lack of HI absorption toward the VLBI nucleus, and the southern (approaching) lobe. Consider the simple example of a constant opening angle disk in which the half width of the disk increases linearly with radial distance from the center, with a constant of proportionality C . The nucleus will be unobscured as long as: $\cotan(i) \leq C$. For instance, if we adopt a value of $i = 45^\circ$ (see section 4.2), then the nucleus and southern (approaching) lobe will be unobscured as long as the disk half width is less than the disk radius at any

given radius. An additional factor in forming the ‘HI hole’ toward the nucleus of Mrk 231 could be ionization of the inner disk by the active nucleus (section 4.2).

The total column density for the HI 21cm absorption line system seen toward the radio continuum disk in Mrk 231 is: $N(\text{HI}) = 6.3 \pm 0.7 \times 10^{19} \times \frac{T_s}{f} \text{ cm}^{-2}$, where T_s is the HI spin temperature and f is the HI covering factor ($f \leq 1$). Assuming a pathlength of order $100 \text{ h}^{-1} \text{ pc}$ through the HI implies an average density of roughly: $n(\text{HI}) \approx 0.3 \times \frac{T_s}{f} \text{ h cm}^{-3}$. The total atomic hydrogen mass in the disk is then of order: $M(\text{HI}) \approx 10^4 \times \frac{T_s}{f} \text{ h}^{-2} \text{ M}_\odot$. The value of T_s is unknown, but typical Galactic values range from 10^2 to 10^4 K (Heiles and Kulkarni 1989). The value of f is also unknown, but if the radio continuum emitting regions are co-spatial with the atomic gas (section 4.2), then $f \approx 0.5$.

Bryant and Scoville (1996) estimate a minimum H_2 mass in Mrk 231 of about 10^9 M_\odot within a radius of $300 \text{ h}^{-1} \text{ pc}$, with an average H_2 column density of 10^{23} cm^{-2} . Roche and Chandler (1993) show that the sub-mm and infrared spectrum of Mrk 231 can be reasonably fit by a model of a dust disk with a diameter of about $0.4''$ and a temperature of 85 K . This disk would be optically thick even in the far IR, with a minimum total dust mass of $8 \times 10^9 \text{ M}_\odot$. Lastly, from the free-free opacity toward the northern radio lobe in Mrk 231, Ulvestad et al. (1997a) estimate an emission measure of $2 \times 10^7 \text{ pc cm}^{-6}$ toward the northern lobe, implying a thermal electron column density of 10^{23} cm^{-2} on a scale of 20 mas .

If the spin temperature of the neutral hydrogen is fairly high ($\geq 10^3 \text{ K}$), then the column densities in the ionized, neutral atomic, and molecular material are all of order 10^{23} cm^{-2} , with the different components being detected on increasing scales. This leads to the interesting speculation that perhaps we are seeing the transition from an ionized inner disk at radii $\leq 20 \text{ h}^{-1} \text{ pc}$, to a neutral atomic disk at radii between $20 \text{ h}^{-1} \text{ pc}$ and $100 \text{ h}^{-1} \text{ pc}$, to a mostly molecular and dusty disk at radii between $100 \text{ h}^{-1} \text{ pc}$ and $300 \text{ h}^{-1} \text{ pc}$ (Figure 9). Using the rough value for the mean $n(\text{HI})$ given above, and assuming a neutral gas

temperature of 10^4 K, the implied Stromgren radius is: $r_{st} = 25 \times [\frac{L_{uv}}{10^{44}}]^{1/3} \text{ h}^{-2/3} \text{ pc}$, where L_{uv} is the AGN luminosity above 13.6 eV in ergs s^{-1} .

The dynamical mass can be estimated assuming that the HI is in a Keplerian rotating disk. The observed velocity at a radius of $50 \text{ h}^{-1} \text{ pc}$ is about 110 km s^{-1} . Hence, the enclosed mass inside this radius is: $M_{dyn} = 1.4 \times 10^8 \text{ h}^{-1} (\sin i)^{-2} M_{\odot}$. Assuming that $i \approx 45^\circ$ (see section 4.2), leads to $M_{dyn} = 3 \times 10^8 \text{ h}^{-1} M_{\odot}$. Note that the HI absorption line FWHM of 180 km s^{-1} seen by the shorter spacings of our VLBI observations is comparable to the value seen for the integrated CO emission from Mrk 231. Given the different maximum radii sampled in these two observations ($120 \text{ h}^{-1} \text{ pc}$ versus $360 \text{ h}^{-1} \text{ pc}$), this similarity in line widths suggests that the rotation curve of the disk could be flat, or falling, at radii larger than about $100 \text{ h}^{-1} \text{ pc}$. In this case, we can set an upper limit to the velocity dispersion in the disk of $\approx 140 \text{ km s}^{-1}$, and using the equations of hydrostatic equilibrium (Scoville et al. 1997), we can set an upper limit to the effective thickness of the disk of 30 pc . For comparison, Scoville et al. (1997) derive a velocity dispersion for the disk in Arp 220 of 90 km s^{-1} , from which they derive a disk thickness of 16 kpc .

4.2. The Synchrotron Emitting Disk

The diffuse radio continuum component seen by the shorter VLBA spacings (Figure 3) is elliptical with a major axis orientation the same as that seen for the molecular gas (east-west), although on a factor three smaller scale. The major-to-minor axis ratio for this diffuse radio component is about 1.4, which is also similar to that of the CO disk. It is plausible, therefore, to assume that this radio continuum emission is associated with the disk. For a circular, flat disk, the observed axis ratio implies a disk orientation angle relative to the sky plane of 45° .

The radio continuum ‘disk’ in Mrk 231 has a brightness temperature of 10^6 K, suggesting non-thermal emission, ie. synchrotron radiation. One possible origin for the relativistic electrons is first order Fermi acceleration in supernova remnant shocks due to massive star formation in the disk. The proposed physical conditions in the disk are certainly conducive to star formation (Bryant and Scoville 1996, Scoville et al. 1997). A diagnostic as to whether star formation is a reasonable explanation for the radio continuum emission from the disk is the IR-to-radio flux density ratio: $Q \equiv \log \left[\frac{S_{100} + 2.6 \times S_{60}}{3 \times S_{1.4}} \right]$ (Condon 1992), where $S_{1.4}$ is the radio continuum flux density at 1.4 GHz in Jy, and S_{60} and S_{100} are the IR flux densities at $60 \mu\text{m}$ and $100 \mu\text{m}$, respectively, also in Jy. The majority of the IR emission from Mrk 231 comes from a region with a scale comparable to that of the radio continuum disk (Roche and Chandler 1993, Mathews et al. 1987), with flux densities of: $S_{60} = 35$ Jy, and $S_{100} = 32$ Jy (Soifer et al. 1989). The radio continuum emission from the disk has: $S_{1.4} = 0.13$ Jy, leading to a value of: $Q = 2.5$. This value is consistent with the tight correlation seen for starburst galaxies, for which $Q = 2.3 \pm 0.2$ (Condon 1992). The implied massive star formation rate is $60 \text{ M}_{\odot} \text{ year}^{-1}$ in the disk for stars with mass $\geq 5 \text{ M}_{\odot}$ using the empirical relations given in Condon (1992).

The minimum pressure in the relativistic particles and magnetic fields in the radio continuum disk of Mrk 231 is about $3 \times 10^{-9} \text{ dynes cm}^{-2}$, with corresponding magnetic fields of order $300 \mu\text{G}$. While this pressure is much higher than typical interstellar pressures in our galaxy, it is comparable to pressures hypothesized in the nuclei of some nearby starburst galaxies (Carilli 1996, Heckman et al. 1990). Also, this pressure is still a factor of a few below that hypothesized by Bryant and Scoville (1996) in the self-gravitating disk in Mrk 231. The synchrotron and inverse Compton radiative lifetimes for the relativistic particles emitting at 1.4 GHz in the disk of Mrk 231 are $< 10^5$ years. Streaming velocities for relativistic electrons in the interstellar medium are thought to be limited to the Alfvén speed due to scattering off self-induced Alfvén waves (Wentzel 1974). Assuming a mean

thermal particle density of order 10^3 cm^{-3} implies an Alfvén speed of order 20 km s^{-1} , leading to a streaming distance less than a few pc in the particle lifetime. Hence *in situ* particle acceleration may be required, such as could occur eg. in supernova remnant shocks (Condon et al. 1991).

The physical conditions for the thermal and non-thermal gas in the sub-kpc disk of Mrk 231 are similar to those proposed for compact nuclear starburst galaxies by Condon et al. (1991). In a sample of 39 IR luminous galaxies, Condon et al. find that about a third show evidence for a nuclear starburst region with star formation rates $\geq 10 \text{ M}_\odot \text{ year}^{-1}$ on scales of only a few hundred parsecs. They propose that the sources are optically thick in the IR, and that the free-free opacities can be significant at cm wavelengths. The expected supernova rates are about one per year, leading to very high interstellar pressures in these regions ($\approx 10^8 \text{ dyne cm}^{-2}$). A potential problem with interpreting the disk in Mrk 231 as a compact starburst region of the type seen by Condon et al. is the high radio continuum brightness temperature of 10^6 K at 1.4 GHz. Condon et al. use an empirical scaling relation between thermal and non-thermal radio continuum emission based on more extended starburst galaxies to set an upper limit to the allowed brightness temperature in a compact starburst of 10^5 K at 1.4 GHz assuming a thermal electron temperature of 10^4 K . A possible solution to this problem is to hypothesize that the empirical scaling relations break down under the extreme conditions in compact starbursts. An argument against this solution is the fact that these regions obey the standard radio-IR correlation for starburst galaxies. Alternatively, one could arbitrarily raise the thermal electron temperature by an order of magnitude, or else assume that the relativistic electrons are not accelerated in supernova remnant shocks. A possible alternative particle acceleration mechanism is stochastic (second order) Fermi acceleration in a turbulent disk.

Recent observations have supported the hypothesis of sub-kpc gas disks in the nuclei

of two other galaxies. Scoville et al. (1997) have used high resolution CO observations to infer a molecular disk in the ULIRG Arp 220 with a mass, size, and velocity structure similar to that seen in Mrk 231. They suggest that the disk is fairly thin, with a diameter of 220 pc and a scale height of 16 pc, based on the observed line widths and assuming hydrostatic equilibrium. While they find it difficult to model the IR emission from Arp 220 via star formation alone, they also point out that, given the physical conditions in the disk, it would be hard to avoid active star formation, perhaps at a rate as high as $90 \text{ M}_{\odot} \text{ year}^{-1}$. Mundell et al. (1995) have proposed a gaseous disk in the nucleus of the Seyfert II galaxy NGC 4151, although on a factor of a few smaller scale than the disk in Mrk 231, based on high resolution HI 21cm observations (see also Ulvestad et al. 1997c, and Silver, Taylor, and Vermeulen 1997).

Figure 9 shows a schematic diagram of the model presented above to explain the various observations of the nuclear regions of Mrk 231. We hypothesize a gaseous disk comprised of multiple phases: (i) ionized atomic gas, as seen in free-free absorption on scales $\approx 20 \text{ h}^{-1} \text{ pc}$, (ii) neutral atomic gas, as seen in HI 21cm absorption on scales $\approx 120 \text{ h}^{-1} \text{ pc}$, (iii) relativistic gas, as seen in radio continuum emission on scales $\approx 240 \text{ pc}$, and (iv) molecular gas and dust, as seen in CO and infrared emission on scales $\approx 600 \text{ h}^{-1} \text{ pc}$.² This disk is centered on the AGN, and is oriented at about 45° from the sky plane, and the radio jet axis is oriented perpendicular to the disk. The southern (brighter) pc-scale radio lobe is approaching, and hence is unobscured by the disk. In order to have an unobscured view into the nucleus (in terms of HI 21cm absorption), the inner disk opening half-angle must be less than the angle of the disk relative to our light sight (45°), although ionization of the inner disk by the AGN could weaken this constraint. In this model the neutral

²Note that the scales quoted above are set mainly by observational limitations, and hence the data do not preclude a mixture of the various gaseous phases on different scales.

atomic gas is roughly co-spatial with the diffuse radio continuum disk, thereby giving rise to the HI 21cm absorption seen by the VLA and the shorter VLBI baselines, while at the same time the radio nucleus and the southern pc-scale lobe are not obscured by the HI disk. The diffuse radio continuum emission from the disk is likely to be driven by distributed massive star formation. An upper limit to the velocity dispersion in the disk provides an upper limit to the disk effective thickness of 30 pc.

4.3. The Temperature of the BAL Gas

No HI 21cm absorption has been detected in the velocity range of the optical low ionization BAL systems. The strongest and broadest of the BAL systems toward Mrk 231 is the one at $cz = 8000 \text{ km s}^{-1}$. This optical system has been analyzed extensively by Forster et al. (1995), who find that the broad NaI line can be reasonably fit by a blend of nine unsaturated absorbing clouds with a total velocity spread of 840 km s^{-1} , with optical depths varying between 0.1 and 1.5, and Doppler parameters between 50 km s^{-1} and 70 km s^{-1} . The implied NaI column density in each component is about: $N(\text{NaI}) = 2 \times 10^{13} \text{ cm}^{-2}$, with the strongest component having a column density of $6 \times 10^{13} \text{ cm}^{-2}$.

Our 3σ neutral hydrogen column density limit towards this system is: $N(\text{HI}) \leq 1.3 \times 10^{18} \frac{T_s}{f} \text{ cm}^{-2}$. If the BAL gas has a solar abundance of NaI, then the implied HI column density would be: $N(\text{HI}) = 3.6 \times 10^{19} \times d \text{ cm}^{-2}$, where d is the dust depletion factor ($d \geq 1$). The implied lower limit to the spin temperature is then: $T_s \geq 30 \times d \times f \text{ K}$. Boksenberg et al. have hypothesized that the two magnitudes of visual extinction toward the nucleus of Mrk 231 is due to the broad absorption line systems. If this is the case, then one might expect $d \approx 10$ (Spitzer 1978). Alternatively, assuming a Galactic dust-to-gas ratio, the observed value of $A_v = 2$ implies a total $N(\text{HI}) = 3.2 \times 10^{21} \text{ cm}^{-2}$. Dividing this equally among the nine velocity components, and comparing the result to the HI 21cm

absorption measurements leads to a lower limit to the HI spin temperature of: $T_s \geq 275 \times f$ K. Note that the BAL gas must cover at least the active nucleus, which sets a lower limit: $f > 0.2$, based on the VLBI imaging results, leading to $T_s > 50$ K.

Given the detection of low ionization species such as NaI and CaII in the BAL systems toward the nucleus of Mrk 231, we had hoped to detect HI 21cm absorption. The negative results in the radio require that the neutral atomic gas be fairly warm, unless the NaI abundance is higher than solar, or the dust-to-gas ratio is higher than Galactic, or the observed extinction toward the nucleus of Mrk 231 is not due to the BAL gas.

5. Summary

Our imaging with the VLBA of the neutral hydrogen 21cm absorption line system seen toward the nuclear regions of Mrk 231 has shown that the absorption is not toward the radio core or lobes seen on pc-scales, but that the absorption occurs against a more diffuse radio continuum component seen on a scale of a few hundred parsecs. A plausible explanation for these data is that both the HI 21cm absorption and the radio continuum emission occur in a disk centered on the active galactic nucleus. The disk cannot be oriented too far from the sky plane, or else the nucleus would show HI 21cm absorption, and the pc-scale radio lobe source must be oriented close to the axis of the disk. The radio continuum morphology is consistent with a disk of maximum radius of 440 mas ($260 \text{ h}^{-1} \text{ pc}$) at an inclination angle of 45° , with a major axis oriented east-west. The HI 21cm absorption shows an east-west gradient in position and velocity of about $\pm 110 \text{ km s}^{-1}$ out to radii $\approx 100 \text{ mas}$ ($60 \text{ h}^{-1} \text{ pc}$). The parameters for the morphology of this disk (orientation of the major axis and inclination angle), and the observed HI velocity field, are very similar to those seen for the self-gravitating molecular gas disk discovered by Bryant and Scoville (1996) in Mrk 231, although on a factor three smaller scale. We would then identify the observed neutral

atomic and radio continuum emitting disk with the inner regions of the molecular disk seen in CO emission.

The physical conditions for the thermal and non-thermal gas in the sub-kpc disk of Mrk 231 are similar to those proposed for compact nuclear starburst galaxies (Condon et al. 1991), and in particular to the conditions proposed for the sub-kpc gas disk in Arp 220 (Scoville, Yun, and Bryant 1997). The minimum pressure in the non-thermal gas is 3×10^{-9} dynes cm^{-2} , with corresponding magnetic fields of order $300 \mu\text{G}$. The IR-to-radio flux density ratio for the disk implies a value of $Q = 2.5$, consistent with the tight correlation seen for starburst galaxies. The implied massive star formation rate in the disk is $60 M_{\odot} \text{ year}^{-1}$. From the neutral hydrogen velocity field we derive a gravitational mass enclosed within a $50 h^{-1} \text{ pc}$ radius of $3 \times 10^8 h^{-1} M_{\odot}$. We propose that Mrk 231 provides a relatively nearby example of the physical processes and conditions seen in high redshift ULIRGs (Scoville, Yun, and Bryant 1996).

We also present a search for HI 21cm absorption associated with the optical broad absorption line (BAL) systems seen toward Mrk 231. We do not detect HI 21cm absorption associated with any of the optical BAL systems. The 3σ optical depth limit is 0.009 for the systems at $cz = 4660 \text{ km s}^{-1}$ and 6250 km s^{-1} , with a velocity resolution of 21 km s^{-1} . The limit for the broadest system at 8000 km s^{-1} is 0.008 at a velocity resolution of 84 km s^{-1} . These negative results require that the neutral atomic gas in the BAL clouds be fairly warm ($T_s > 50 \text{ K}$), unless the NaI abundance is higher than solar, or the dust-to-gas ratio is higher than Galactic, or the observed extinction toward the nucleus of Mrk 231 is not due to the BAL gas.

We thank Min Su Yun, Alan Roy, and Greg Taylor for useful comments and discussions. This research made use of the NASA/IPAC Extragalactic Data Base (NED) which is operated by the Jet propulsion Lab, Caltech, under contract with NASA. The National

Radio Astronomy Observatory is a facility of the National Science Foundation operated under cooperative agreement by Associated Universities, Inc.

References

- Armus, L., Surace, J.A., Soifer, B.T., Matthews, K., Graham, J.R., and Larkin, J.E. 1994, A.J., 108, 76
- Bocksenberg, A., Carswell, R.F., Allen, D.A., Fosbury, R.A., Penston, M.V., and Sargent, W.L.W. 1977, M.N.R.A.S. 178, 451
- Boroson, T.A., Meyers, K.A., Morris, S.L., and Persson, S.E. 1991, Ap.J. (letters), 370, L19
- Bryant, P.M. and Scoville, N.Z. 1996, Ap.J., 457, 678
- Carilli, C.L., Perley, R.A., Dreher, J.W., and Leahy, J.P. 1991, Ap.J., 383, 554
- Carilli, C.L. 1996, A.&A., 305, 402
- Clark, B.G. 1980, A&A, 89, 377
- Condon, J.J. 1992, A.R.A.A., 30, 575
- Condon, J.J., Huang, Z.P., Yin, Q.F., and Thuan, T.X. 1991, Ap.J. 378, 65
- Dickey, J. 1982, Ap.J., 263, 87
- Forster, Karl, Michael, Rich R., and McCarthy, J.K. 1995, Ap.J., 450, 74
- Hamilton, J.B. and Keel, W.C. 1987, Ap.J., 321, 211
- Heckman, T.M., Balick, B., and Sullivan, W.T. 1978, Ap.J. 224, 745
- Heckman, T.M., Armus, L., and Miley, G. 1990, Ap.J. (supplement), 73, 883
- Heiles, C. and Kulkarni, S. 1989, in *Galactic and Extragalactic Radio Astronomy*, eds. K. Kellerman and G. Verschuur (Berlin: Kluwer)
- Hutchings, J.B. and Neff, S.G 1987, A.J., 93, 14

- Kollatschny, W., Dietrich, M., Hagen, H. 1992, A&A (letters), 264, L5
- Matthews, K., Neugebauer, G., McGill, J. and Soifer, B.T. 1987, A.J. 94, 297
- Mundell, C.G., Pedlar, A., Baum, S.A., O’Dea, C.P., Gallimore, J.F., and Brinks, E. 1995, M.N.R.A.S., 272 355
- Napier, P.J., Thompson, A.R., and Ekers, R.D. 1983, Proc. IEEE, 71, 1295
- Napier, P.J., Bagri, D.S., Clark, B.G., Rogers, A.E.E., Romney, J.D., Thompson, A.R., and Walker, R.C. 1994, Proc. IEEE, 82, 658
- Roche, P.F. and Chandler, C.J. 1993, M.N.R.A.S., 265, 486
- Rudy, R.J., Foltz, C.B, and Stocke, J.T. 1985, Ap.J., 288, 531
- Sanders, D.B. and Mirabel, I.F. 1996, A.R.A.A., 34, 749
- Sanders, D.B., Soifer, B.T., Elias, J.H., Madore, B.F., Matthews, K., Neugebauer, G., and Scoville, N.Z. 1988, Ap.J., 325, 74
- Silver, C.S., Taylor, G.B., and Vermeulen, R.C. 1997, Ap.J. (letters), submitted
- Soifer, B.T., Boehmer, L., Neugebauer, G., and Sanders, D.B. 1989, A.J., 98, 766
- Scoville, N.Z., Yun, M.S., and Bryant, P.M. 1997, Ap.J., 484, 702
- Scoville, N.Z., Yun, M.S., and Bryant, P.M. 1996, in *Cold Gas at High Redshift*, eds. M. Bremer, P. van der Werf, H. Röttgering, and C. Carilli (Kluwer: Dordrecht), p. 25
- Spitzer, Lyman 1978, *Physical Processes in the Interstellar Medium*, (New York: Wiley)
- Surace, J.A., Sanders, D.B., Vacca, W.D., Veilleux, S., and Mazzarella, J.M. 1997, Ap.J., in press

Ulvestad, J.S., Wrobel, J.M., and Carilli, C.L. 1997a, in *IAU Colloquium 164: Radio Emission from Galactic and Extragalactic Compact Sources*, eds. G.B. Taylor, J.M. Wrobel & J.A. Zensus (ASP: San Francisco)

Ulvestad, J.S., Wrobel, J.M., and Carilli, C.L. 1997b, in preparation

Ulvestad, J.S., Roy, A.L., Colbert, E.J.M., and Wilson, A.S. 1997c, *Ap.J.*, submitted

Walker, R.C. 1985, in *Aperture Synthesis in Radio Astronomy*, eds. R. Perley, F. Schwab, and A. Bridle (NRAO: Green Bank), p. 189

Weedman, D.W. 1983, *Ap.J.*, 243, 756

Wentzel, D.G. 1974, *A.R.A.A.*, 12, 71

Figure Captions

Figure 1 – An image of Mrk 231 at 1.4 GHz with a resolution of $5''$ made with the VLA from data taken on January 27, 1993. The contour levels are a geometric progression in the square root of two, hence every two contours implies a factor two rise in surface brightness. The first contour level is $0.5 \text{ mJy beam}^{-1}$, and the peak surface brightness is $240 \text{ mJy beam}^{-1}$.

Figure 2 – An image of Mrk 231 at 1.4 GHz with a resolution of $8 \times 6 \text{ mas}$ made with the VLBA from data taken on December 27, 1996. The contour scheme is the same as Figure 1, with the first contour level equal to $0.8 \text{ mJy beam}^{-1}$, and the peak surface brightness equal to 40 mJy beam^{-1} .

Figure 3 – An image of the radio continuum emission from Mrk 231 at 1.4 GHz with a resolution of 60 mas made with the VLBA from data taken on December 27, 1996. A CLEAN component model of the nucleus and pc-scale lobes (100 mJy total) as seen in Figure 2 has been subtracted from the visibilities before imaging. The contour levels are: 1, 2, 3, 4, 5, 6, 7, 8 mJy beam^{-1} , and the peak surface brightness is $8.2 \text{ mJy beam}^{-1}$. The crosses mark the positions of the nucleus, southern lobe, and northern lobe as seen in Figure 2.

Figure 4 – The HI 21cm absorption spectrum of Mrk 231 made with the VLA on August 31, 1997. The zero point on the velocity scale corresponds to a heliocentric redshift of 0.04217 ± 0.000015 , or $cz = 12642 \pm 4 \text{ km s}^{-1}$. The spatial resolution is $18''$ and the spectral resolution is $10.7 \text{ km s}^{-1} \text{ channel}^{-1}$. The upper plot shows the absorbed flux density, after subtracting the continuum flux density of 242 mJy , and fitting a linear baseline to off-line channels. The lower plot shows the same spectrum converted to optical depth using the continuum flux density. The dashed-line is a one component Gaussian model fit with a peak opacity of 0.083 ± 0.002 , and a velocity FWHM = $179 \pm 5 \text{ km s}^{-1}$.

Figure 5 – The HI 21cm absorption spectra toward the pc-scale VLBI components in Mrk 231 made with the VLBA on December 27, 1996. The zero point on the velocity scale corresponds to a heliocentric redshift of 0.04217 ± 0.000015 , or $cz = 12642 \pm 4 \text{ km s}^{-1}$. The spatial resolution is 13 mas and the spectral resolution is $56 \text{ km s}^{-1} \text{ channel}^{-1}$. The upper plot shows the optical depth spectrum toward the peak surface brightness of the nucleus of 43 mJy beam^{-1} . The middle plot shows the optical depth spectrum toward the southern lobe with a surface brightness of 20 mJy beam^{-1} .

Figure 6 – The HI 21cm absorption spectrum toward radio continuum ‘disk’ in Mrk 231 (see Figure 3) made with the VLBA on December 27, 1996. The zero point on the velocity scale corresponds to a heliocentric redshift of 0.04217 ± 0.000015 , or $cz = 12642 \pm 4 \text{ km s}^{-1}$. The spatial resolution is $0.4''$ and the spectral resolution is $28 \text{ km s}^{-1} \text{ channel}^{-1}$. The upper plot shows the absorbed flux density, after subtracting the continuum flux density of 91 mJy, and fitting a linear baseline to off-line channels. The lower plot shows the same spectrum converted to optical depth using the continuum flux density. The dashed-line is a one component Gaussian model fit with a peak opacity of 0.17 ± 0.02 , a velocity FWHM = $193 \pm 25 \text{ km s}^{-1}$, and a velocity centroid of $-21 \pm 12 \text{ km s}^{-1}$.

Figure 7 – Spectral channel images of the HI 21cm absorption toward Mrk 231 made from data taken with the VLBA on December 27, 1996. The channel spacing is 28 km s^{-1} , however the data have been Hanning smoothed to $56 \text{ km s}^{-1} \text{ channel}^{-1}$, hence adjacent channels are not independent. The spatial resolution is 150 mas. Each panel is labeled with the velocity relative to heliocentric redshift of 0.04217 ± 0.000015 , or $cz = 12642 \pm 4 \text{ km s}^{-1}$. The crosses mark the positions of the nucleus, southern lobe, and northern lobe as seen in Figure 2. The contour levels are: -6,-5,-4,-3,-2,-1, 1 mJy beam^{-1} .

Figure 8 – The HI 21cm absorption spectra of the Mrk 231 made with the VLBA on January 27, 1993 with a spatial resolution of $5''$. All the spectra have been converted to

optical depth using a continuum source flux density of 242 mJy. These spectra were made at the velocities of the optical BAL systems seen toward Mrk 231. The upper plot shows the spectrum centered at a heliocentric redshift of $z = 0.01554$ ($cz = 4660 \text{ km s}^{-1}$). The middle plot shows the spectrum centered at a heliocentric redshift of $z = 0.02085$ ($cz = 6250 \text{ km s}^{-1}$). These two spectra have a spectral resolution of 97.6 kHz. The lower plot shows the spectrum centered at a heliocentric redshift of $z = 0.02668$ ($cz = 8000 \text{ km s}^{-1}$), with a spectral resolution of 390.6 kHz.

Figure 9 – A schematic diagram of the model presented in sections 4.1 and 4.2 to explain the various observations of the nuclear regions of Mrk 231. The contours show the radio continuum emission from the pc-scale lobes and nucleus (Figure 2). The line drawing shows the multi-phase gaseous disk: ionized atomic, neutral atomic, relativistic, and molecular gas and dust. Note that the plot is not drawn strictly to scale, and that the annotated values for size scales for the various gas phases are set mainly by observational limitations, ie. the data do not preclude a mixture of the different gaseous phases on different scales. The ‘stars’ indicate possible distributed massive star formation in the disk, and the diffuse radio continuum emission from the disk is likely to be driven by this star formation. In this model the neutral atomic gas is roughly co-spatial with the diffuse radio continuum disk, thereby giving rise to the HI 21cm absorption seen by the VLA and the shorter VLBI baselines, while at the same time the radio nucleus and southern (approaching) pc-scale radio lobe are not obscured by the HI disk.

Figure 1

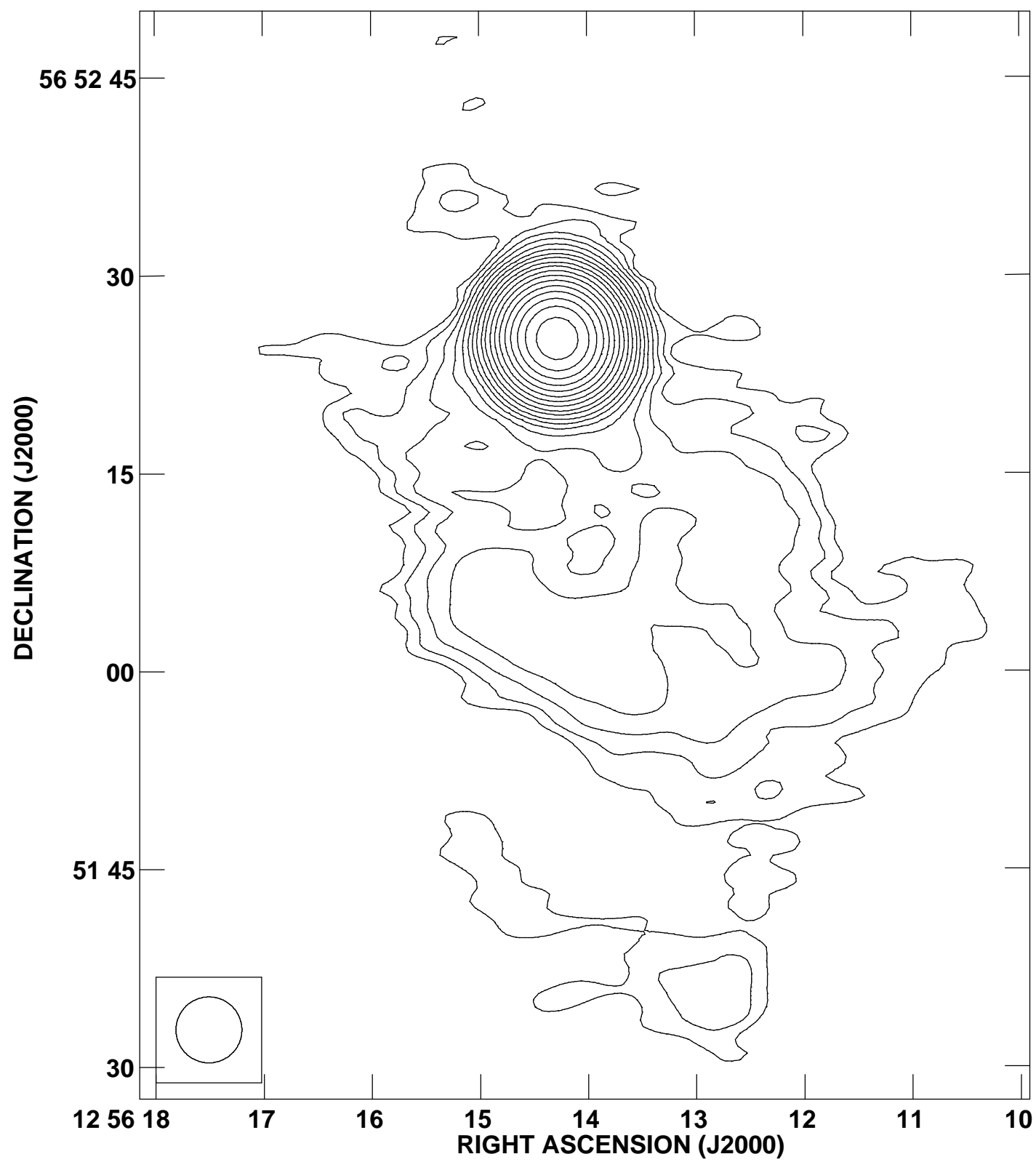


Figure 2

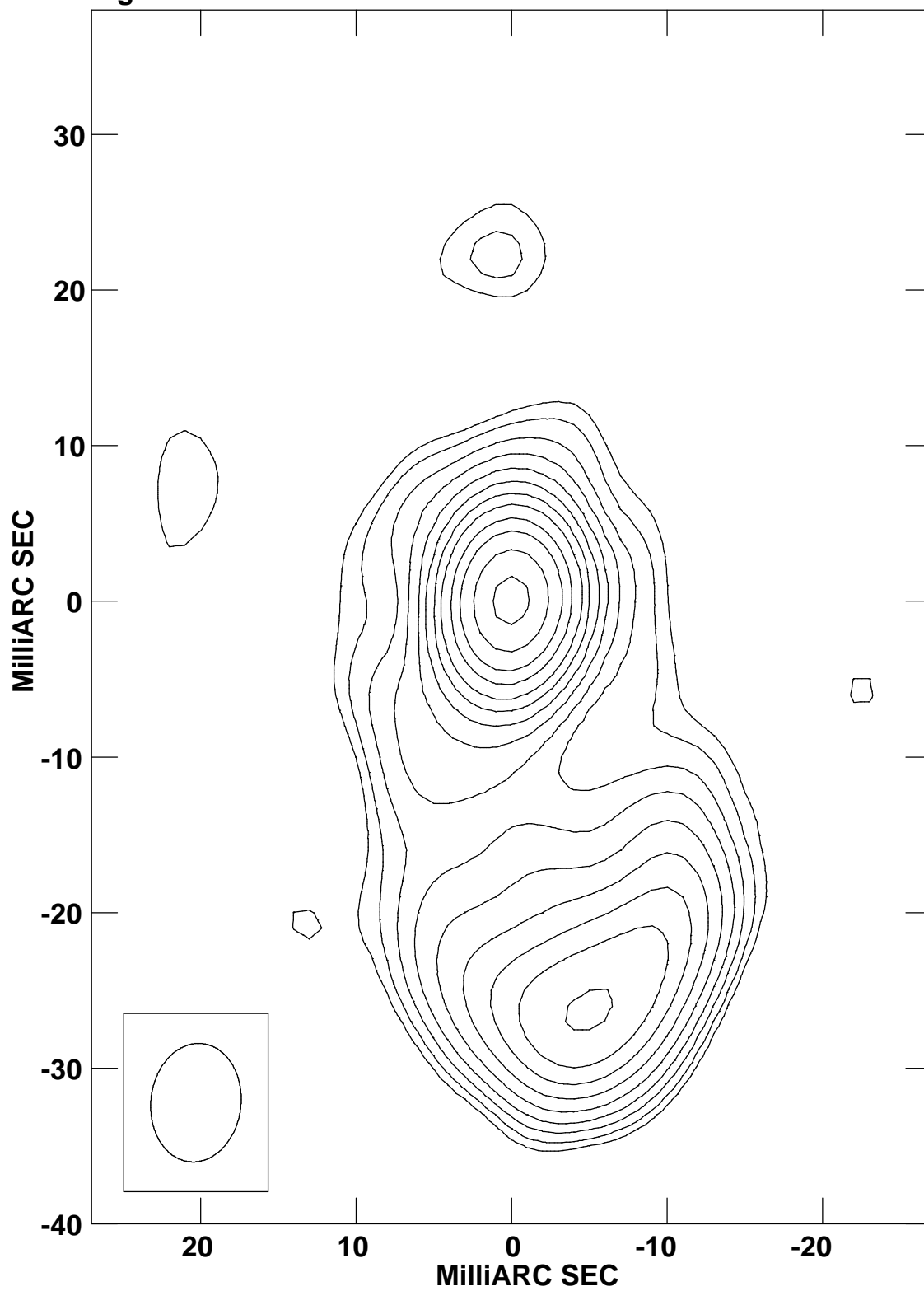


Figure 3

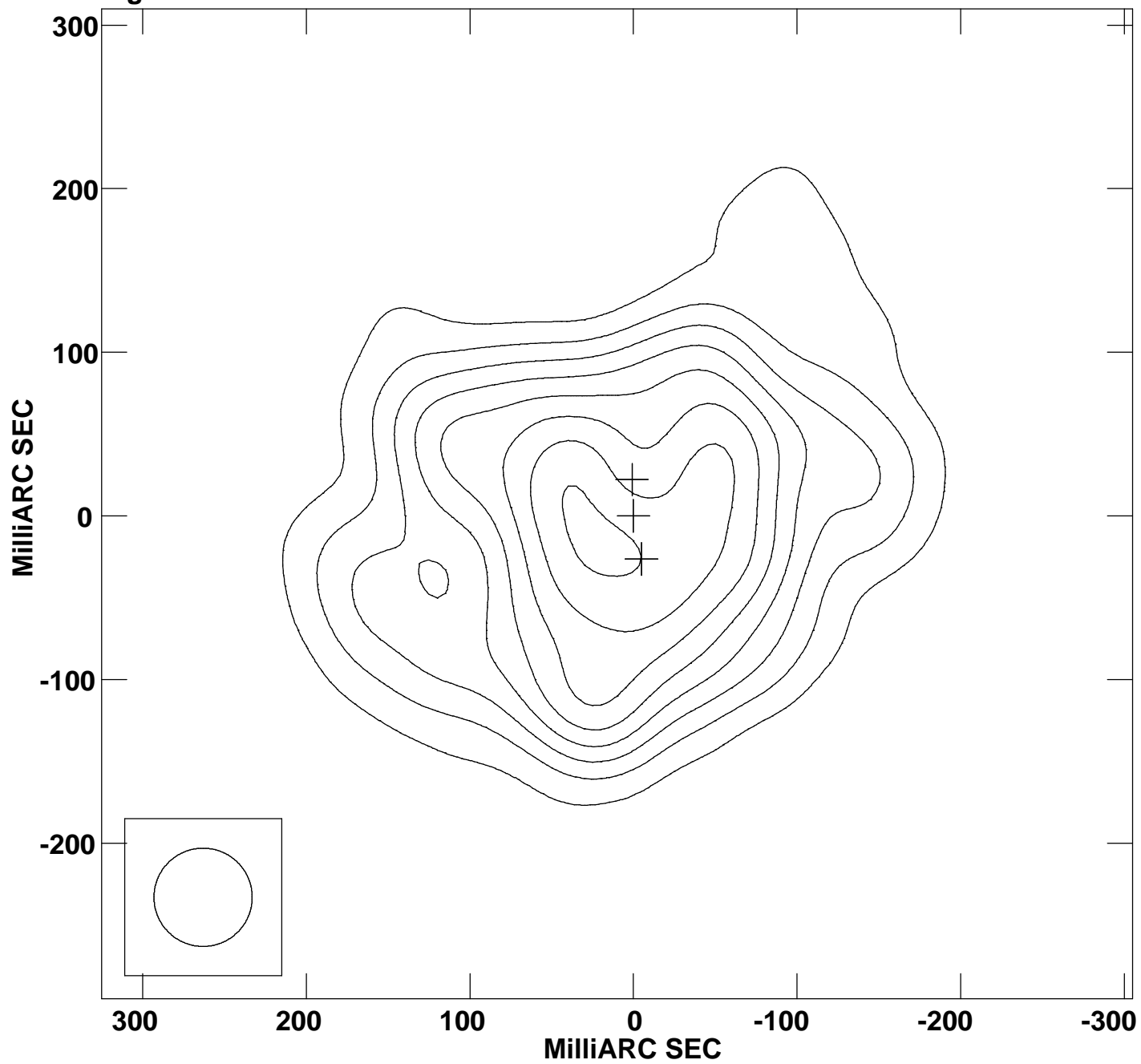


Figure 4

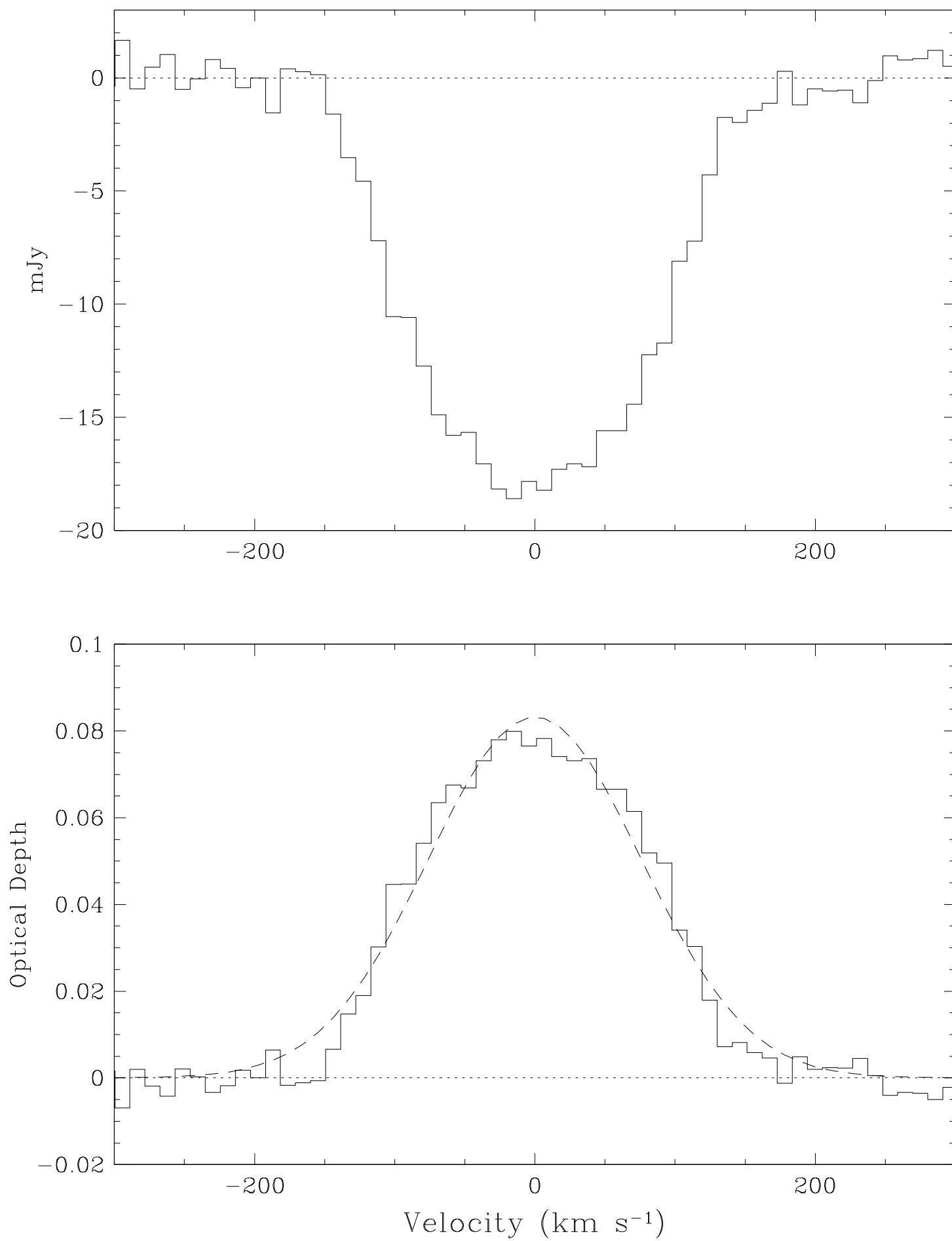


Figure 5

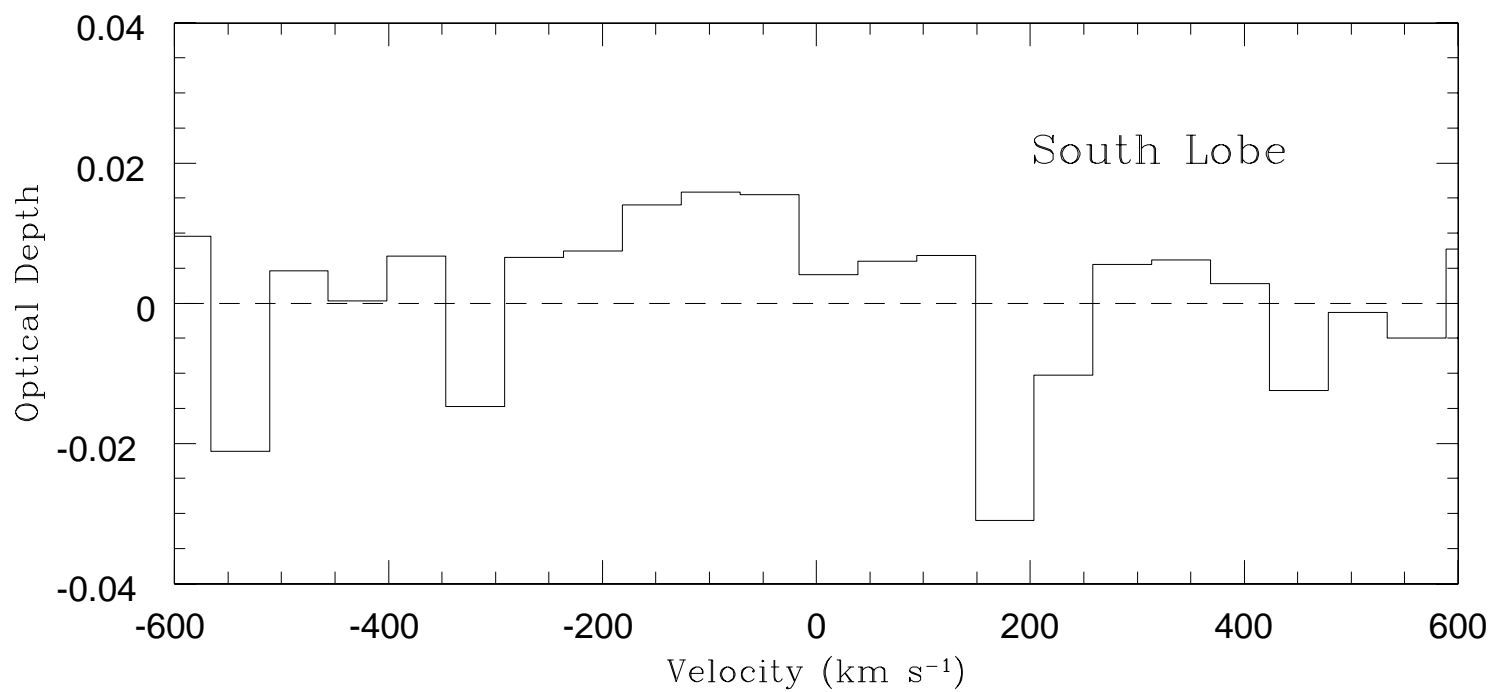
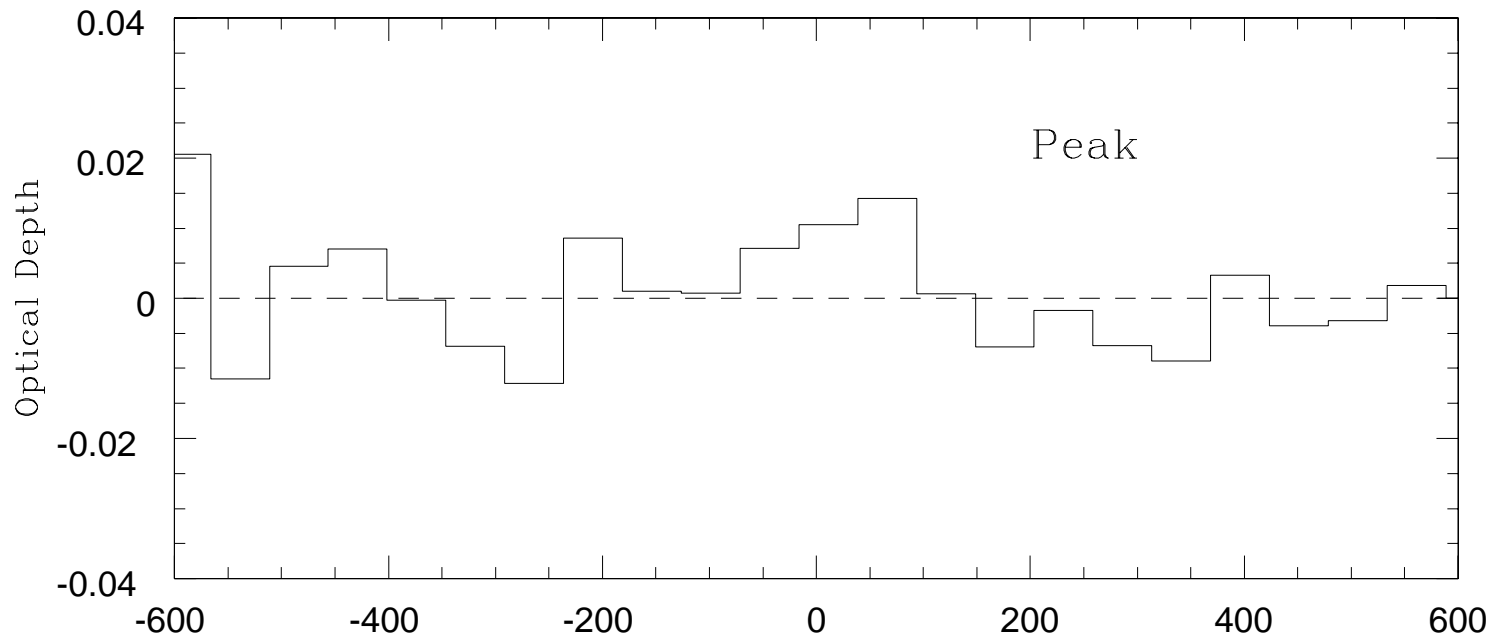


Figure 6

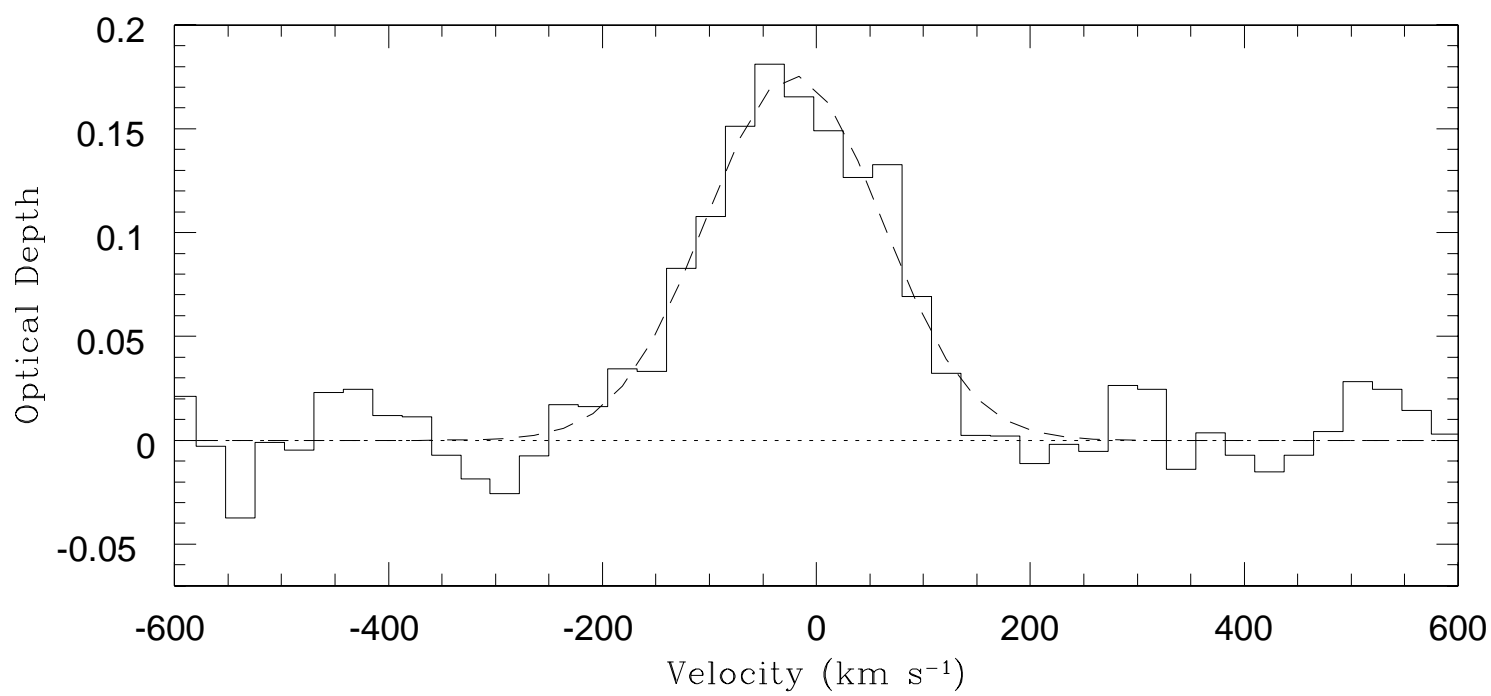
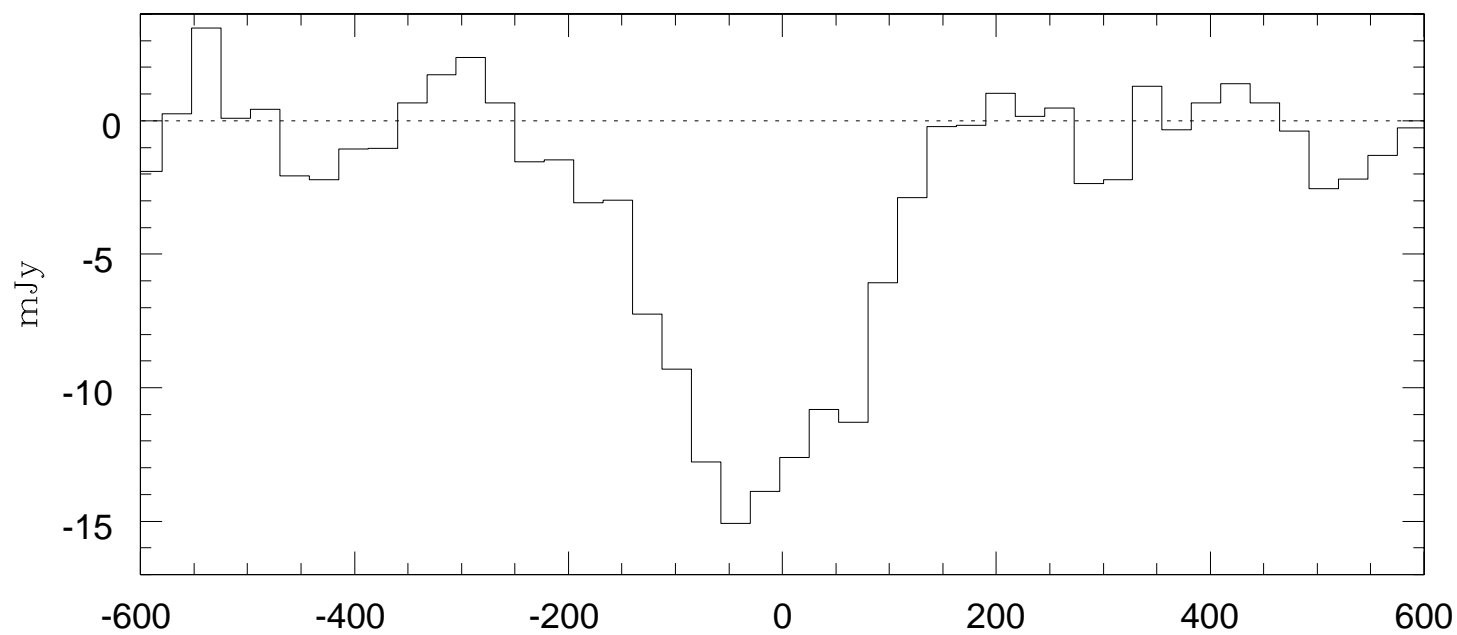


Figure 7

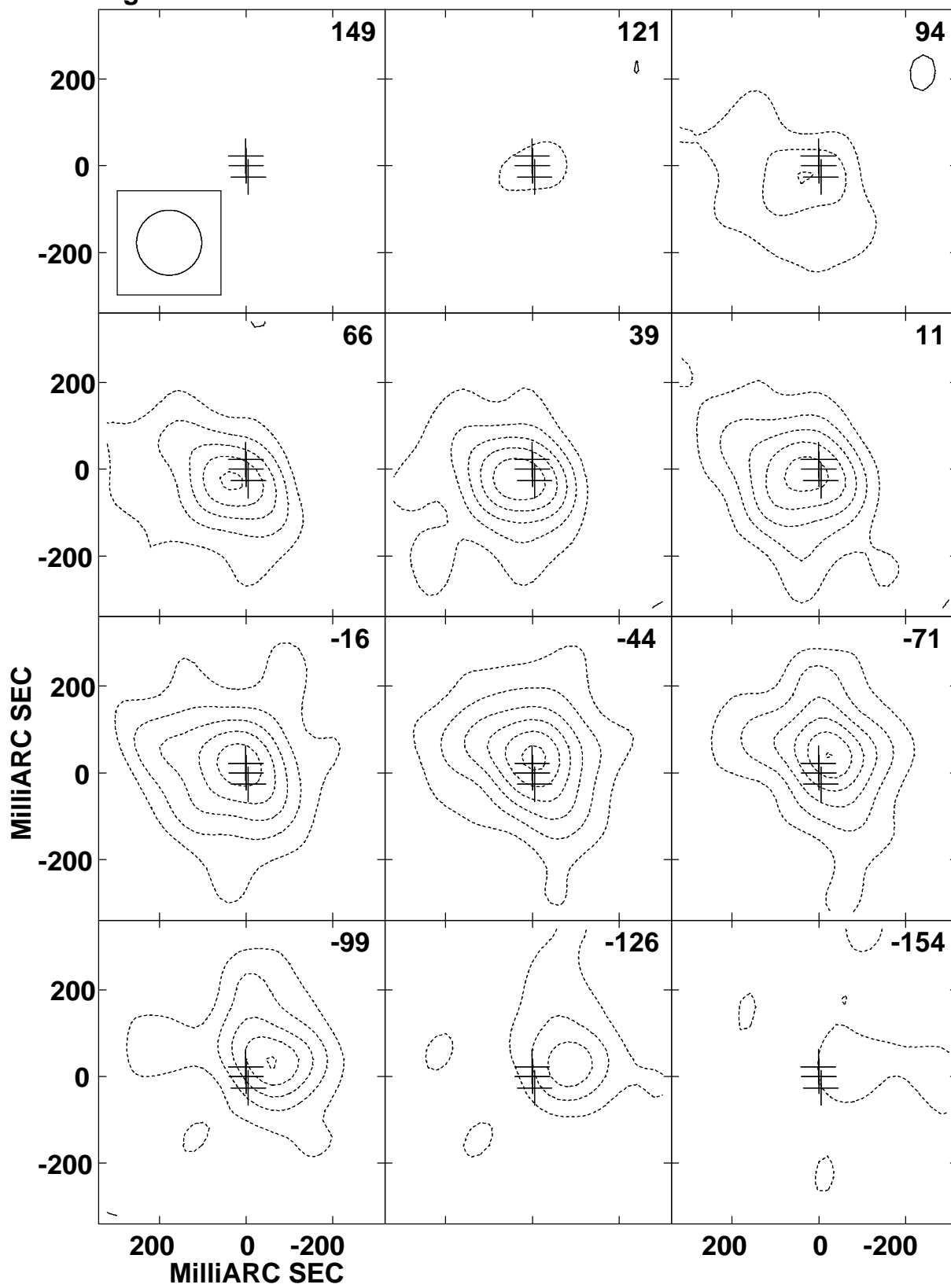


Figure 8

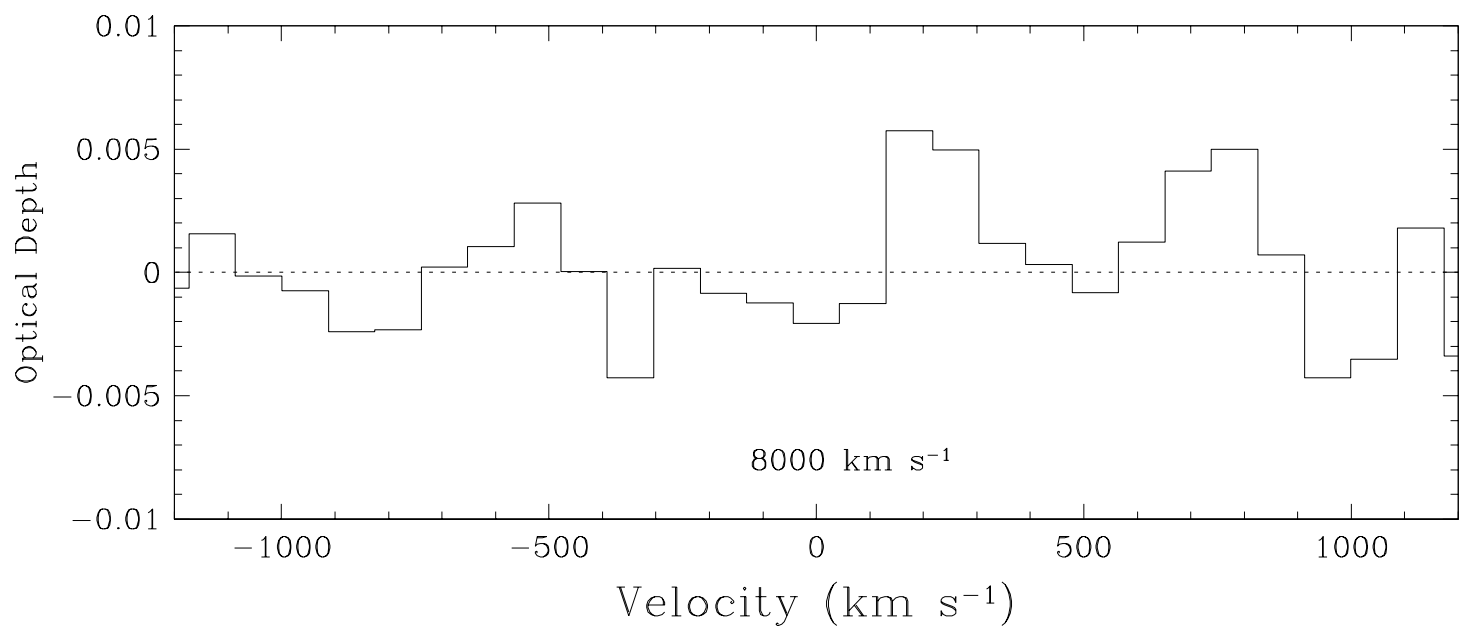
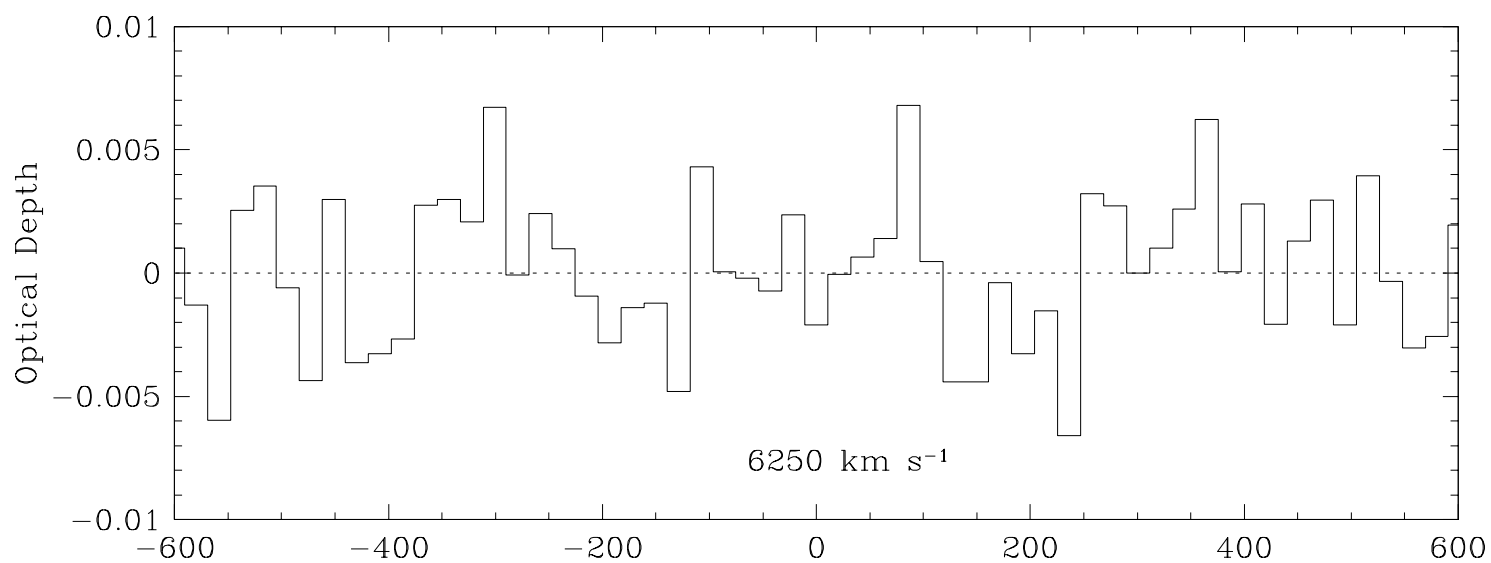
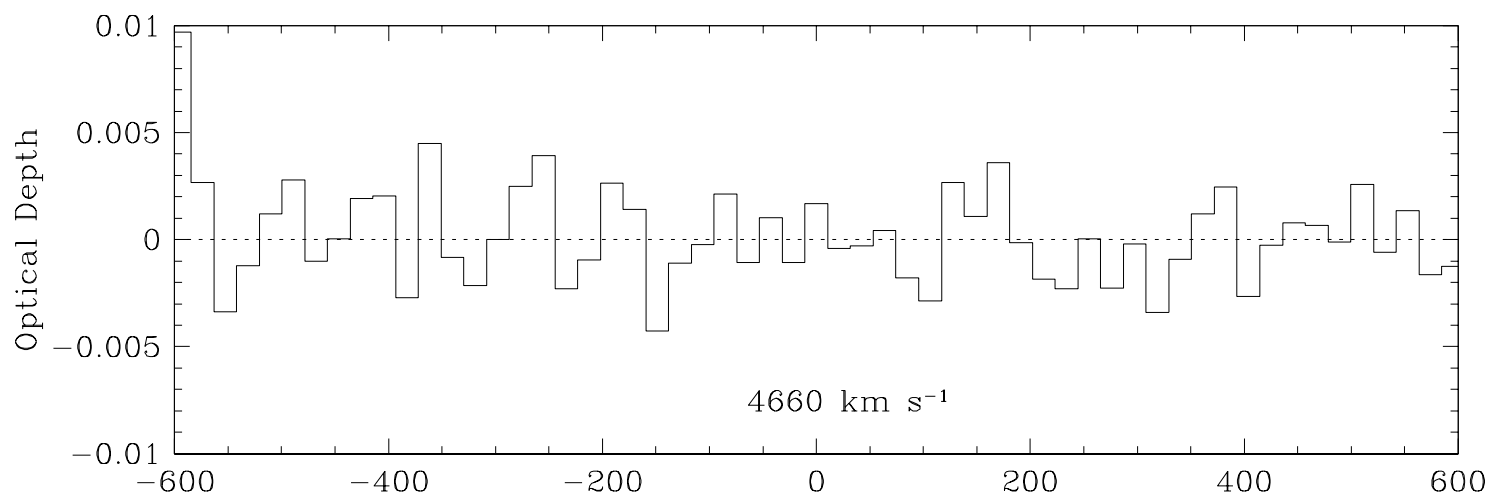


Figure 9 -- Carilli

